

New limits on 2ε , $\varepsilon\beta^+$ and $2\beta^+$ decay of ^{136}Ce and ^{138}Ce with deeply purified cerium sample

P. Belli^{a,b}, R. Bernabei^{a,b,1}, R.S. Boiko^{c,d}, F. Cappella^e, R. Cerulli^f,
 F.A. Danevich^c, A. Incicchitti^{e,g}, B.N. Kropivyansky^c,
 M. Laubenstein^f, V.M. Mokina^{c,e}, O.G. Polischuk^c, V.I. Tretyak^c

^a*INFN sezione Roma "Tor Vergata", I-00133 Rome, Italy*

^b*Dipartimento di Fisica, Università di Roma "Tor Vergata", I-00133 Rome, Italy*

^c*Institute for Nuclear Research, 03028 Kyiv, Ukraine*

^d*National University of Life and Environmental Sciences of Ukraine, 03041 Kyiv, Ukraine*

^e*INFN sezione Roma, I-00185 Rome, Italy*

^f*INFN, Laboratori Nazionali del Gran Sasso, I-67100 Assergi (AQ), Italy*

^g*Dipartimento di Fisica, Università di Roma "La Sapienza", I-00185 Rome, Italy*

Abstract

A search for double electron capture (2ε), electron capture with positron emission ($\varepsilon\beta^+$), and double positron emission ($2\beta^+$) in ^{136}Ce and ^{138}Ce was realized with a 465 cm³ ultra-low background HP Ge γ spectrometer over 2299 h at the Gran Sasso underground laboratory. A 627 g sample of cerium oxide deeply purified by liquid-liquid extraction method was used as a source of γ quanta expected in double β decay of the cerium isotopes. New improved half-life limits were set on different modes and channels of double β decay of ^{136}Ce and ^{138}Ce at the level of $T_{1/2} > 10^{17} - 10^{18}$ yr.

Keywords: Double beta decay, ^{136}Ce , ^{138}Ce , Radiopurity of materials, Low background experiment, HP Ge γ spectrometry

¹Corresponding author. *E-mail address:* rita.bernabei@roma2.infn.it (R. Bernabei).

1. Introduction

A great interest in double beta (2β) decay is motivated by the observation of neutrino oscillations phenomena. The neutrinoless (0ν) mode of 2β decay is forbidden in the Standard Model of particles since the process violates the lepton number and requires neutrino to be a massive Majorana particle [1–4]. In addition to the massive neutrino mechanism, there are a lot of other hypothetical mechanisms of the $0\nu 2\beta$ decay [5, 6].

The two neutrino double beta minus ($2\nu 2\beta^-$) processes, allowed in the Standard Model, are already observed in several nuclei, while the half-life limits set on the 0ν mode achieved in the most sensitive experiments are at level of $T_{1/2} > 10^{23} - 10^{26}$ yrs (see reviews [3, 7–12] and the recent experimental results [13–17]). The experiments bound the effective Majorana neutrino mass at the level of 0.1 eV – a few eV depending on experiment and on the nuclear matrix elements calculations, which still give a rather wide spread of values. The experimental sensitivity to the double beta plus processes: double electron capture (2ε), electron capture with positron emission ($\varepsilon\beta^+$), and double positron emission ($2\beta^+$) is substantially lower. Even the allowed two neutrino mode of these processes has not yet been observed unambiguously (see reviews [7, 18]). At the same time, there is a strong motivation to enhance the experimental sensitivity to the $0\nu 2\varepsilon$ and $0\nu\varepsilon\beta^+$ decay processes since these investigations could clarify the possible contribution of the right-handed currents to the $0\nu 2\beta^-$ decay rate if observed [19].

For neutrinoless double electron capture, the so-called resonant mechanism was discussed, when the energy release is very close to the energy of one of the excited levels of the daughter nucleus (see [20–22] and references therein). In the other case, to save the energy-momentum conservation, it is supposed that the energy excess is taken away by emission of one or two gamma quanta, conversion electron or e^+e^- pair (see e.g. [23]).

The isotope ^{136}Ce is one of the most promising double beta plus nuclei thanks to the high energy of the decay ($Q_{2\beta} = 2378.55 \pm 0.27$ keV [24]) and a comparatively high decay probability. However, the isotopic abundance of ^{136}Ce is rather low: $\delta = 0.186 \pm 0.002\%$ [25], which is typical for the double beta plus active isotopes: their concentration in the natural isotopic composition of elements is usually less than 1%. A simplified decay scheme of ^{136}Ce is shown in Fig. 1. Due to the large decay energy ^{136}Ce is among the most studied nuclei. Double beta processes in the cerium isotopes were searched for by using scintillation counting [26–29] and γ spectrometric [30,

31] methods. In the present study we use an ultra-low background HP Ge γ spectrometer to search for γ quanta of certain energies expected in de-excitation of daughter nuclei, that is the signature of the events under search.

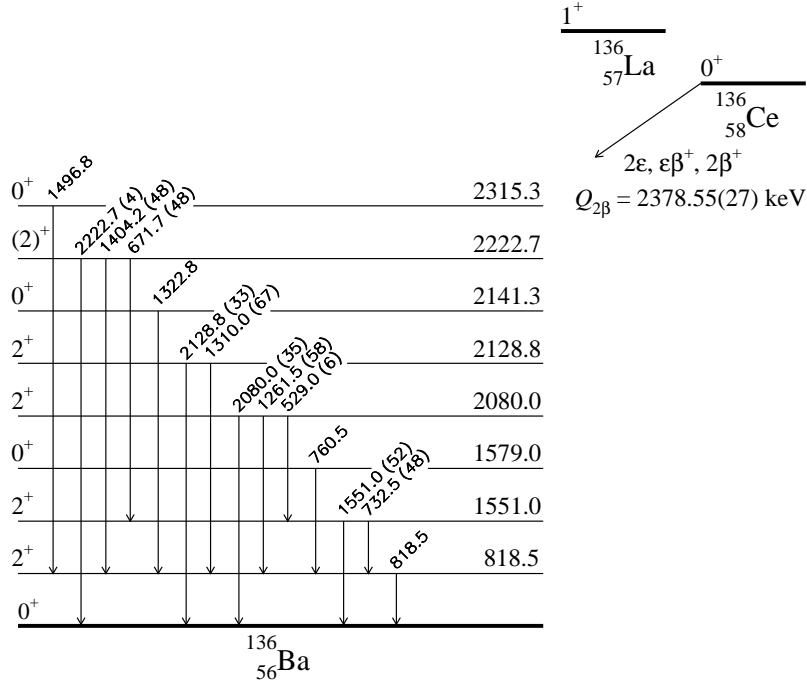


Figure 1: The simplified decay scheme of ^{136}Ce . Energy of the levels and γ quanta are in keV, the transition probabilities (in %) are given in parentheses.

Cerium contains two other potentially double beta active isotopes: ^{138}Ce ($Q_{2\beta} = 691 \pm 5$ keV [24], $\delta = 0.251 \pm 0.002\%$ [25]), the decay scheme is presented in Fig. 2) and ^{142}Ce ($Q_{2\beta} = 1416.8 \pm 2.2$ keV [24], $\delta = 11.114 \pm 0.051\%$ [25]). The last isotope is out of the present study since no γ quanta are expected in its 2β decay.

In Section 2 we describe the purification of the cerium oxide sample. The experimental set-up and the radioactive contamination of the sample after the purification will be reported in Section 3. It should be stressed that deep purification of cerium is also motivated in the light of radiopure crystal scintillators development. Cerium can be used to develop Ce-containing crystal scintillators (as for instance, CeF_3 and CeCl_3), and as a dopant in inorganic scintillators: $\text{Gd}_2\text{SiO}_5(\text{Ce})$, $\text{YAlO}_3(\text{Ce})$, $\text{LaBr}_3(\text{Ce})$, etc. The analysis of the

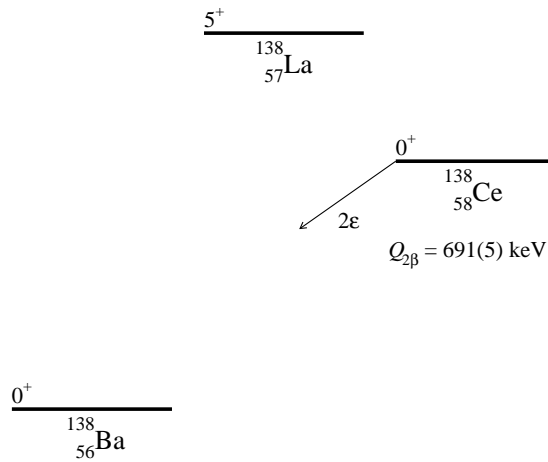


Figure 2: Decay scheme of ^{138}Ce .

data, collected by using a sample of purified cerium oxide in a HP Ge detector, and the obtained limits on 2β processes in ^{136}Ce and ^{138}Ce are reported in Sect. 4.

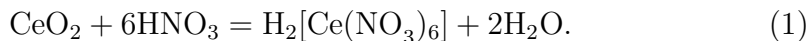
2. Purification of cerium

Cerium oxide of 99% TREO purity grade ($\text{CeO}_2/\text{TREO} - 99.99\%$) was provided by the Stanford Materials Corporation and purified as described in [31]. However, the concentration of thorium remained rather high [31] (see also columns 3 and 4 of Table 1). The contamination by thorium (along with radium) has a major impact on 2β experiments sensitivities. Thus, we decided to perform an additional purification of the material (called 2nd purification in Table 1). The purification of the cerium oxide was performed by using the liquid-liquid extraction method already successfully applied for a variety of rare earths purification from radioactive contamination [32]. The purification has reduced the thorium concentration in the sample by a factor of ≈ 60 , that allowed to improve the sensitivity of the experiment to the 2ε , $\varepsilon\beta^+$ and $2\beta^+$ decay of ^{136}Ce by one order of magnitude. The purification protocol is described in the following.

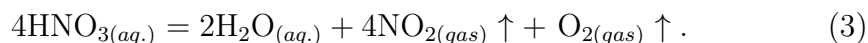
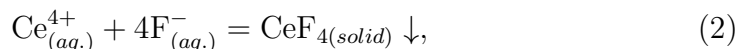
2.1. Cerium aqueous solution preparation

Ultra-pure nitric and hydrofluoric acids solutions were used to dissolve the CeO_2 powder to obtain a homogeneous aqueous solution. The initial mixture

ratios were calculated to achieve both maximum cerium concentration and high acidity of the solution. Very little additions of hydrofluoric acid and heating of the system initiated the following process:



At the same time two parallel reactions occur, which decrease the concentrations of cerium and nitric acid:



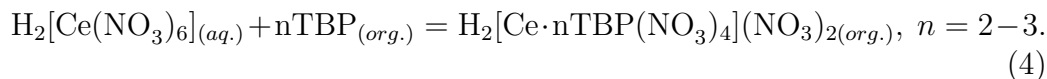
The final solution composition was determined as 1.1 mol·L⁻¹ of Ce⁴⁺ and 11.7 mol·L⁻¹ of HNO₃.

2.2. Preparation of organic extracting TBP liquid

Tributyl phosphate (TBP, Acros Organics, 99+%) has been chosen as the most investigated solvent-extraction agent for lanthanides separation. To decationize the organic liquid, 2 mol·L⁻¹ nitric acid solutions were prepared from ultra-pure HNO₃ and deionized water (18.2 MΩ·cm at 25 °C) and then stirred for several minutes with an equal volume of TBP. The residual aqueous solution was thrown away due to the complete immiscibility of the phases, and the organic liquid was rinsed with deionized water three times in a similar way.

2.3. Extraction of cerium

The extraction of cerium from the aqueous solution to the organic phase of TBP can be described as:

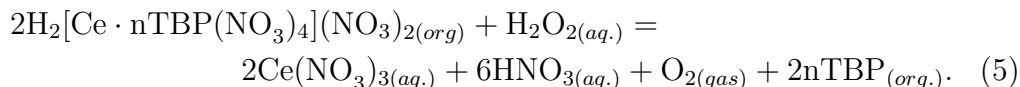


The competitive extraction of the cation impurities K⁺, Ra²⁺, and lanthanides (Ln³⁺) at the same conditions should be very low, practically zero. However, Th⁴⁺ has the same chemical behavior as Ce⁴⁺, thus it is extracted in a similar way. Taking into account the initial cerium concentration and stoichiometry in reaction (4), the liquid ratio was taken 1(aq.) to 0.75(org.) on volume basis. The two liquids were mixed together in a separation funnel,

stirred for 2–3 minutes and left for phase separation. After that, the organic liquid was separated. The extraction degree has been determined to be 84%.

2.4. Re-extraction of cerium

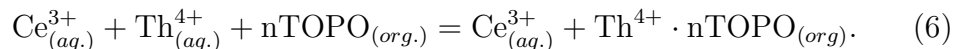
After separation of the cerium contained organic solution in the previous step, 0.1 M HNO₃ aqueous solution was used as re-extracting liquid. Simultaneous reduction of Ce⁴⁺ to Ce³⁺ by hydrogen peroxide addition was utilized to decrease the distribution ratio between "organic" and "aqueous" cerium:



The volumetric ratio of the two phases was 1 to 1. The re-extraction of uranium is negligible at these conditions while the removal of tetravalent thorium from organic to aqueous phase can be explained by formation of an insoluble colloid thorium peroxide compound. After the re-extraction procedure, the obtained aqueous solution was heated for a while to decompose the thorium peroxide and the hydrogen peroxide in excess. The determined re-extraction degree of cerium was 65% with respect to the initial cerium oxide amount.

2.5. Extraction of thorium

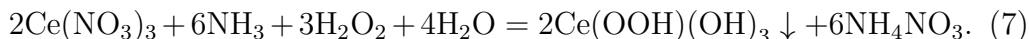
Low acidic tri-*n*-octylphosphine oxide diluted to a concentration of 0.1 mol·L⁻¹ in toluene has been used as extraction agent for Th⁴⁺ ions from the aqueous solution containing cerium:



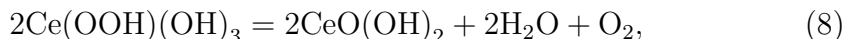
The volumetric ratio was 1 of inorganic (aqueous) to 0.5 of organic phase. However, Ce³⁺ does not leave the inorganic phase in this process (6). After the separation of the phases, the final purified cerium solution was prepared for the last step of cerium oxide recovery.

2.6. Cerium oxide recovery from solution

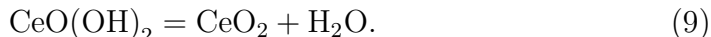
The acidic cerium (III) nitrate solution was neutralized with ammonia gas to reach a pH level up to 7. The residual presence of hydrogen peroxide from the "cerium re-extraction" step caused the chemical oxidation of Ce^{3+} to Ce^{4+} in the low-acidic media that resulted in precipitation of cerium hydroxyperoxide:



The obtained amorphous sediment was decomposed by heating it over 4 – 6 hours at 90 °C:



and separated from the liquid phase by using a centrifuge. The final cerium oxide solid was prepared by annealing the $\text{CeO}(\text{OH})_2$ at 900 °C for 6 hours:



As a result, 627 g of deeply purified CeO_2 were obtained that is about 62% of the initial amount of the material.

3. Low counting experiment

The sample of deeply purified cerium oxide with mass 627 g, encapsulated in a thin plastic container with internal sizes $\varnothing 90 \times 50$ mm, was placed on the endcap of a high purity germanium (HP Ge) detector named GeCris, with an active volume of 465 cm^3 , in the STELLA facility at the Laboratori Nazionali del Gran Sasso. The detector is shielded by low radioactive lead (≈ 25 cm), copper (≈ 5 cm), and in the innermost part by Roman lead (≈ 2.5 cm). The set-up is enclosed in an air-tight PMMA box and permanently flushed with High Purity boiling-off nitrogen to reduce the radon concentration. The energy resolution of the detector (full width at half maximum, FWHM) depends on the energy E_γ of the γ quanta as $\text{FWHM}(\text{keV}) = \sqrt{1.41 + 0.00197 \times E_\gamma}$, where E_γ is in keV.

The energy spectrum measured by the HP Ge detector with the CeO_2 sample over 2299 h is presented in Fig. 3 together with background data accumulated over 1046 h. The counting rate in the energy spectrum measured

with the CeO₂ sample is substantially lower than that after the first stage of the material purification [31]. There is some excess in the CeO₂ data due to the residual contamination of the sample, mainly by radium (²²⁸Ra). Activities of radionuclides in the CeO₂ sample (A) were estimated by using the following formula:

$$A = (S_{sample}/t_{sample} - S_{bg}/t_{bg})/(\eta_{\gamma} \cdot m), \quad (10)$$

where S_{sample} (S_{bg}) is the area of a peak in the sample (background) spectrum; t_{sample} (t_{bg}) is the time of the sample (background) measurement; η_{γ} is the detection efficiency of γ quanta in the full absorption peak; m is the mass of the sample. The detection efficiencies were estimated by Monte Carlo simulations with EGSnrc [33] and GEANT4 [34] packages as well as the event generator DECAY0 [35, 36]. Both the codes give compatible values of the detection efficiencies for γ quanta of ⁴⁰K, ¹³⁷Cs, ¹³⁸La, ¹³⁹Ce, ¹⁵²Eu, ¹⁵⁴Eu, ¹⁷⁶Lu and γ -emitting daughters of ²³²Th, ²³⁵U and ²³⁸U. The efficiencies calculated by GEANT4 and EGSnrcs differ on average in $\sim 3\%$, with a maximal difference 12.7% (for the low intensity γ quanta 1001.0 keV of ^{234m}Pa from the ²³⁸U chain). The EGSnrcs code systematically gives slightly bigger efficiencies. The statistical errors of the Monte Carlo calculations are within 0.5%–0.6%. We have used weighted mean values of the detection efficiencies obtained by the two codes to calculate the activities (or upper limits) of contaminants in the CeO₂ sample, since we have not found arguments to prefer one of the codes. The detection efficiencies include the branching ratios for the γ quanta incorporated in the DECAY0 event generator [35, 36]. The upper limits were set in the cases when the values and errors of the difference ($S_{sample} - S_{bg} \cdot t_{sample}/t_{bg}$) give no signature of the γ peak observation. The results of the CeO₂ sample radiopurity analysis are presented in Table 1.

4. Results for 2β processes and discussion

Gamma quanta of certain energies are expected in de-excitation of daughter nuclei in the 2β processes in ¹³⁶Ce and ¹³⁸Ce according to the decay schemes (Figs. 1 and 2). We suppose that, in result of ¹³⁶Ce decay, some excited level (or the ground state) of ¹³⁶Ba is populated with 100% probability. In the subsequent de-excitation process, probabilities of transitions to different lower levels with emission of γ quanta (or conversion electrons or e^+e^- pairs) are taken from [37]. All these probabilities are incorporated in

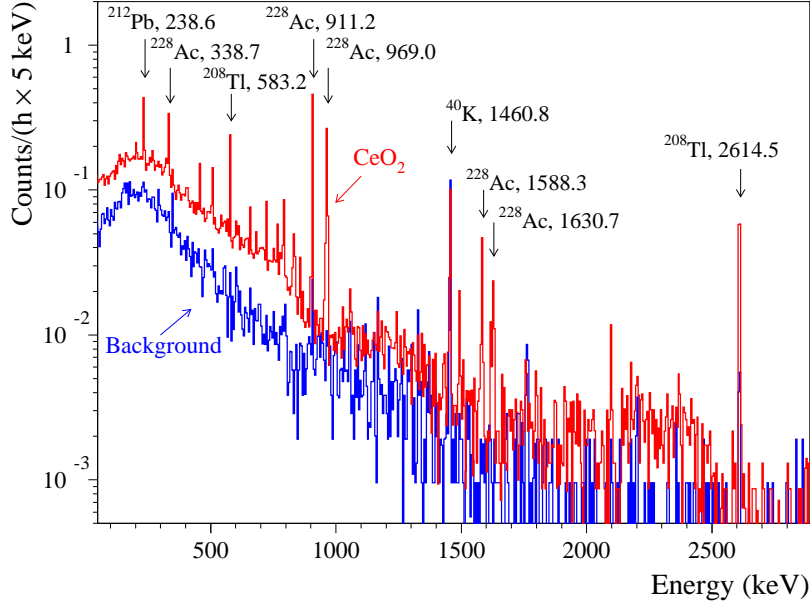


Figure 3: Energy spectra measured by the GeCris HP Ge detector with cerium oxide sample (CeO_2) over 2299 h and background accumulated over 1046 h (Background). The counting rate in the energy spectrum accumulated with the CeO_2 sample is substantially lower in comparison to the previous experiment (see Fig. 3 in [31]) thanks to the deep purification of the material described in Section 2. Some excess in the CeO_2 data is mainly due to the residual contamination of the sample by radium (^{228}Ra). Energy of γ quanta are in keV.

the DECA0 event generator [35, 36]. In neutrinoless 2ε process, the emission of one quantum with energy $E_\gamma = Q_{2\beta} - E_{exc} - E_{b_1} - E_{b_2}$ is supposed, where E_{exc} is the energy of the excited level, and E_{b_i} is the binding energy of the i -th captured electron on the atomic shell.

Since there are no peculiarities in the spectrum of the CeO_2 sample, which could be ascribed to the 2β decay of ^{136}Ce or ^{138}Ce , we have calculated lower half-life limits using the following formula:

$$\lim T_{1/2} = N \cdot \eta \cdot t \cdot \ln 2 / \lim S, \quad (11)$$

where N is the number of ^{136}Ce or ^{138}Ce nuclei in the CeO_2 sample, η is the detection efficiency, t is the measuring time, and $\lim S$ is the number of events of the effect searched for which can be excluded at a given confidence level (C.L.). The CeO_2 sample contains 4.06×10^{21} and 5.51×10^{21} nuclei of

Table 1: Radioactive contamination of the cerium oxide before and after two stages of purification. The reference date for the activities of the CeO₂ sample after the 2nd purification is April 12, 2016. Upper limits are given at 90% C.L., the uncertainties of the measured activities are given at 68% C.L.

Chain	Nuclide	Activity (mBq kg ⁻¹)		
		before purification [31]	after 1st purification [31]	after 2nd purification
	⁴⁰ K	77(28)	≤ 9	≤ 4
	¹³⁷ Cs	≤ 3	≤ 2	0.4 ± 0.2
	¹³⁸ La	–	≤ 0.7	≤ 0.6
	¹³⁹ Ce	–	6 ± 1	1.4 ± 0.3
	¹⁵² Eu	–	≤ 0.5	≤ 0.2
	¹⁵⁴ Eu	–	≤ 0.9	≤ 0.08
	¹⁷⁶ Lu	–	≤ 0.5	0.4 ± 0.1
²³² Th	²²⁸ Ra	850 ± 50	53 ± 3	30.4 ± 0.7
	²²⁸ Th	620 ± 30	573 ± 17	9.8 ± 0.5
²³⁵ U	²³⁵ U	38 ± 10	≤ 1.8	≤ 0.4
	²³¹ Pa	–	≤ 24	≤ 0.4
	²²⁷ Ac	–	≤ 3	≤ 1.4
²³⁸ U	²³⁸ U	≤ 870	≤ 40	≤ 12
	²²⁶ Ra	11 ± 3	≤ 1.5	≤ 0.3

¹³⁶Ce and ¹³⁸Ce, respectively. The full absorption peak detection efficiencies of the set-up to the γ quanta expected in the double beta decay of ¹³⁶Ce and ¹³⁸Ce were calculated using the EGSnrc and GEANT4 packages together with the event generator DECAY0. The efficiencies calculated by GEANT4 and EGSnrcs differ on average in $\sim 1.5\%$ with a maximal difference 5.7% (the EGSnrcs code again gives higher efficiencies). The statistical errors of all the calculations are within 0.3% – 0.6%. Thus, as in the contamination analysis, we have used weighted mean values of the detection efficiencies. The detection efficiencies are given in Table 2.

The sensitivity of the experimental set-up to the $2\nu 2\varepsilon$ decay of ¹³⁶Ce

and ^{138}Ce is almost negligible due to the very low detection efficiency of the detector for the X rays expected in the decays. Thus, we omit estimations on these decay half-lives.

In the case of double electron capture in ^{136}Ce to the excited states of ^{136}Ba , γ quanta can be detected with reasonable efficiencies at a level of a few %. The parts of energy spectrum collected with the CeO_2 sample in the vicinity of the expected γ quanta 760.5 keV, 818.5 keV and 1551.0 keV of the 2ε decays of ^{136}Ce to the excited states of ^{136}Ba are shown in Fig. 4. A fit of the data in the energy interval 745 – 767 keV was done by using a model consisting of three Gaussian functions and a polynomial function of the 1st degree is used to express the continuous background. Two Gaussian functions describe the γ peaks in the vicinity of the energy of interest: 755.3 keV (^{228}Ac) and 763.1 keV (^{208}Tl), while the third one with energy 760.5 keV describes the peak expected in the 2ε decay of ^{136}Ce to the 0^+ 1579 keV excited level of ^{136}Ba (the fit function is shown in Fig. 4). The positions and energy resolutions of the peaks were fixed according to the expected energies and the measured dependence of the HP Ge detector energy resolution on energy of γ quanta. The fit gives an area of the 760.5 keV peak $S = 8.0 \pm 6.9$ counts (the quality of the fit is characterized by the value of $\chi^2/\text{n.d.f.} = 1.55$), that is no evidence on the effect searched for. An upper limit $\text{lim } S = 19.3$ counts was obtained by using the Feldman-Cousins procedure [38].

However, taking into account a more favorable background condition in the vicinity of the expected 818.5 keV peak, and almost the same detection efficiency ($\eta = 2.31\%$ for 760.5 keV and $\eta = 2.60\%$ for 818.5 keV γ quanta), the analysis of 818.5 keV line is more sensitive to the 2ε decays of ^{136}Ce to the 0^+ 1579 keV excited state of ^{136}Ba . We have used the following model of background in the energy interval 775 – 835 keV: a polynomial function of the 1st degree to describe the continuous background, γ peaks at energies 782.0 keV, 785.5 keV, 795.0 keV, and 830.4 keV (γ quanta of ^{228}Ac and ^{212}Bi , see Fig. 4) and the 818.5 keV peak searched for. We should use such a complicated model to describe the background in the vicinity of the energy 818.5 keV correctly. The fit gives area of the peak $S = -1.5 \pm 4.9$ counts ($\chi^2/\text{n.d.f.} = 1.47$). Since this value gives no evidence for the effect searched for, we have estimated the number of events which can be excluded at 90% C.L. as $\text{lim } S = 6.6$ counts using the approach given in [38]. The excluded peak is shown in Fig. 4. Thus, the lower limit could be increased by almost one order of magnitude with respect to the previous experiment [31]. The new lower bound on the half-life of the two neutrino double electron capture

in ^{136}Ce to the 0^+ 1579.0 keV excited level of ^{136}Ba is $T_{1/2} \geq 2.5 \times 10^{18}$ yr. The $\text{lim}S$ estimation was used to set limits also for decays to the first 2^+ 818.5 keV, and some other 2ε and $\varepsilon\beta^+$ transitions in ^{136}Ce towards excited levels of ^{136}Ba (see Table 2).

To set a limit on the 1551.0 keV peak we added to the background model also the γ peak of ^{228}Ac with energy 1557.1 keV. The result of the fit is shown in the lower panel of Fig. 4. Limits on other double electron capture processes in ^{136}Ce to the excited levels of ^{136}Ba , presented in Table 2, were set in a similar way.

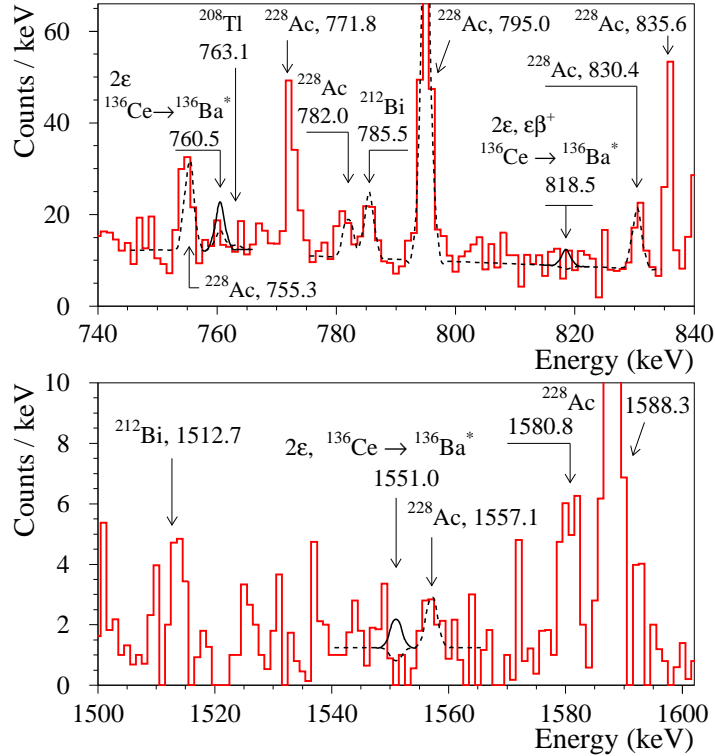


Figure 4: Energy spectrum measured with cerium oxide sample (CeO_2) over 2299 h in the energy intervals where γ peaks with energies 760.5 keV, 818.5 keV and 1551.0 keV are expected. The excluded peaks are shown by solid lines, the backgrounds for the processes are shown by dashed lines.

In the case of the 0ν double electron capture in ^{136}Ce and ^{138}Ce from K and L shells to the ground states of the daughter nuclei, the energies of the γ

quanta are expected to be equal to $E_\gamma = Q_{2\beta} - E_{b_1} - E_{b_2}$, where E_{b_i} are the binding energies of the captured electrons on the K and L atomic shells of the daughter nuclei. The energy spectra accumulated with the CeO_2 sample in the vicinity of the expected energies of the quanta for the $0\nu 2\varepsilon$ capture in $^{136,138}\text{Ce}$ to the ground state of $^{136,138}\text{Ba}$ are shown in Fig. 5. In the case of ^{138}Ce $0\nu 2\varepsilon$ decay the energies of the γ quanta are known with an accuracy of ± 5 keV. Therefore, we had to consider larger energy intervals of interest to estimate the limits on the 0ν double electron capture in $^{136,138}\text{Ce}$ from K and L shells. In the case of ^{138}Ce also the peaks of ^{214}Bi with energy 609.3 keV, and of ^{137}Cs with energy 661.7 keV had to be taken into account to build a correct background model in a wide enough energy interval near the expected peaks. The obtained upper limits are given in Table 2.

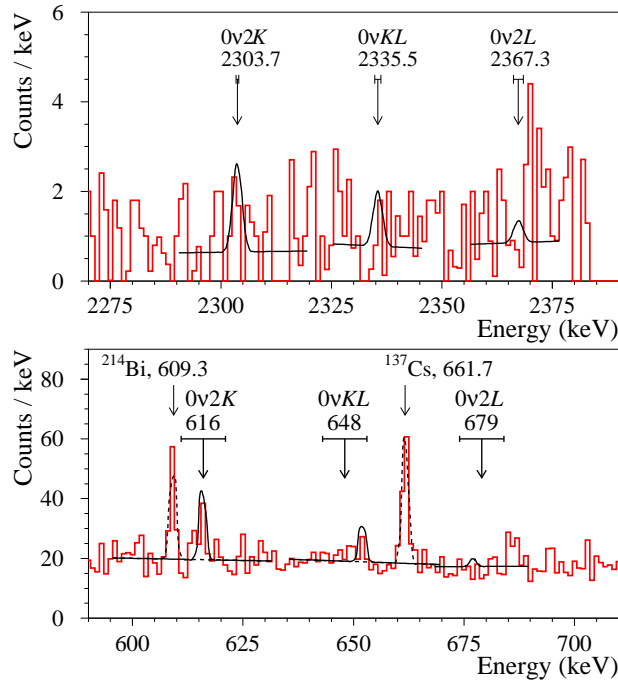


Figure 5: Parts of the energy spectrum collected with the CeO_2 sample where peaks from $0\nu 2\varepsilon$ processes ($2K$, KL and $2L$) in ^{136}Ce (upper panel) and ^{138}Ce (lower panel) are expected. The excluded peaks for the processes are shown by solid lines (the peculiarities providing a maximal area of the expected peak within the interval of interest were considered). The peaks of ^{214}Bi with energy 609.3 keV and of ^{137}Cs with energy 661.7 keV are shown by dashed lines.

The electron capture with positron and double positron emission in ^{136}Ce should lead to the emission of annihilation γ quanta with energy 511 keV. Thus the bounds on the processes were set by analysing the annihilation γ peak in the data taking into account the 511 keV peak in the background and the contributions in this peak from the contaminants present in the sample. The energy spectrum measured with the CeO_2 sample and the background data in the vicinity of the annihilation peak are shown in Fig. 6. Taking into account the radioactive contamination of the CeO_2 by ^{228}Ra and ^{228}Th we have included in the background model the 509.0 keV peak of ^{228}Ac and 510.8 keV peak of ^{208}Tl . The area of the 509.0 + 510.8 + 511 keV peak in the CeO_2 spectrum is 182 ± 26 counts, while the peak in the background data has an area of 20 ± 7 counts (44 ± 14 counts taking into account the different measurements live times). According to the Monte Carlo simulations the radioactivity of ^{228}Ac in the sample provides 33 ± 1 counts in the sum peak, and ^{228}Th contributes 155 ± 8 counts to the annihilation peak. Thus, the difference is -50 ± 31 counts, which corresponds (according to [38]) to $\lim S = 16$ counts at 90% C.L. The estimation leads to the new improved limits on the $\varepsilon\beta^+$ and $2\beta^+$ decays of ^{136}Ce . Again, all the obtained limits on the double beta decay processes in ^{136}Ce and ^{138}Ce are summarized in Table 2.

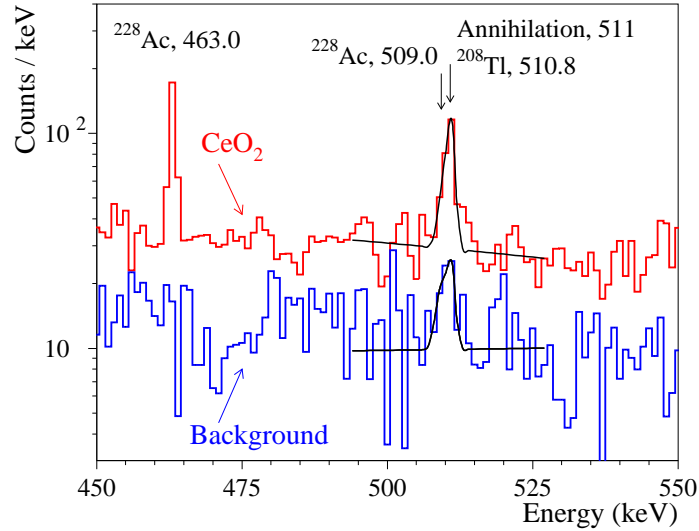


Figure 6: Energy spectrum measured with the cerium oxide sample (CeO_2) over 2299 h and background (1046 h, Background) in the vicinity of the 511 keV annihilation peak.

Table 2: The half-life limits on 2β processes in ^{136}Ce and ^{138}Ce together with the best previous limits and theoretical predictions (the theoretical $T_{1/2}$ values for 0ν mode are given for $m_\nu = 1$ eV). The energies of the γ lines (E_γ), which were used to set the $T_{1/2}$ limits, are listed with their corresponding detection efficiencies (η) and values of $\text{lim } S$.

Process of decay	Decay mode	Level of daughter nucleus (keV)	E_γ (keV)	η (%)	$\text{lim } S$ (cnt) at 90% C.L.	Experimental limits, $T_{1/2}$ (yr) at 90% C.L.		Theoretical estimations, $T_{1/2}$ (yr)
						Present work	Best previous results	
$^{136}\text{Ce} \rightarrow ^{136}\text{Ba}$								
2ε	2ν	2 ⁺ 818.5	818.5	2.60	6.6	$\geq 2.9 \times 10^{18}$	$\geq 3.3 \times 10^{17}$ [31]	–
		2 ⁺ 1551.0	1551.0	1.07	2.3	$\geq 3.4 \times 10^{18}$	$\geq 6.9 \times 10^{17}$ [31]	–
		0 ⁺ 1579.0	818.5	2.26	6.6	$\geq 2.5 \times 10^{18}$	$\geq 1.6 \times 10^{18}$ [31]	–
		2 ⁺ 2080.0	2080.0	0.624	1.64	$\geq 2.8 \times 10^{18}$	$\geq 1.7 \times 10^{18}$ [31]	–
		2 ⁺ 2128.8	2128.8	0.589	3.1	$\geq 1.4 \times 10^{18}$	$\geq 9.1 \times 10^{17}$ [31]	–
		0 ⁺ 2141.3	1322.8	1.84	2.4	$\geq 4.4 \times 10^{18}$	$\geq 2.9 \times 10^{17}$ [31]	–
		(2) ⁺ 2222.7	671.7	1.09	4.1	$\geq 2.0 \times 10^{18}$	$\geq 7.4 \times 10^{17}$ [31]	–
		0 ⁺ 2315.3	818.5	2.26	6.6	$\geq 2.5 \times 10^{18}$	$\geq 2.9 \times 10^{17}$ [31]	–
$2K$	0ν	g.s.	2303.7	1.50	5.2	$\geq 2.1 \times 10^{18}$	$\geq 4.6 \times 10^{17}$ [31]	–
KL	0ν	g.s.	2335.5	1.49	3.2	$\geq 3.4 \times 10^{18}$	$\geq 6.6 \times 10^{17}$ [31]	–
$2L$	0ν	g.s.	2367.3	1.48	1.3	$\geq 8.4 \times 10^{18}$	$\geq 5.4 \times 10^{17}$ [31]	–
2ε	0ν	2 ⁺ 818.5	1485.5	1.73	4.2	$\geq 3.0 \times 10^{18}$	$\geq 2.5 \times 10^{18}$ [31]	–
		2 ⁺ 1551.0	1551.0	0.914	2.3	$\geq 2.9 \times 10^{18}$	$\geq 6.0 \times 10^{17}$ [31]	–
		0 ⁺ 1579.0	818.5	1.95	6.6	$\geq 2.2 \times 10^{18}$	$\geq 1.1 \times 10^{18}$ [31]	–
		2 ⁺ 2080.0	2080.0	0.580	1.64	$\geq 2.6 \times 10^{18}$	$\geq 1.6 \times 10^{18}$ [31]	–
		2 ⁺ 2128.8	818.5	1.43	6.6	$\geq 1.6 \times 10^{18}$	$\geq 8.6 \times 10^{17}$ [31]	–
		0 ⁺ 2141.3	1322.8	1.76	3.12	$\geq 4.2 \times 10^{18}$	$\geq 2.8 \times 10^{17}$ [31]	–
		(2) ⁺ 2222.7	671.7	1.09	4.10	$\geq 2.0 \times 10^{18}$	$\geq 7.3 \times 10^{17}$ [31]	–
		0 ⁺ 2315.3	818.5	2.26	6.6	$\geq 2.5 \times 10^{18}$	$\geq 2.9 \times 10^{17}$ [31]	$1.0 \times 10^{23} - 2.3 \times 10^{33}$ [21, 39, 40]
$\varepsilon\beta^+$	2ν	g.s.	511	5.90	16	$\geq 1.0 \times 10^{17}$	$\geq 2.7 \times 10^{18}$ [31]	$(6.0-28) \times 10^{23}$ [19, 41, 42]
		2 ⁺ 818.5	511	5.16	16	$\geq 2.4 \times 10^{18}$	$\geq 2.5 \times 10^{17}$ [31]	–
	0ν	g.s.	511	5.68	16	$\geq 2.6 \times 10^{18}$	$\geq 9.6 \times 10^{16}$ [31]	$(2.7 - 4.7) \times 10^{26}$ [19, 43, 44]
$2\beta^+$	2ν	g.s.	511	5.09	16	$\geq 2.3 \times 10^{18}$	$\geq 2.5 \times 10^{17}$ [31]	–
		2 ⁺ 818.5	511	5.09	16	$\geq 2.3 \times 10^{18}$	$\geq 2.5 \times 10^{17}$ [31]	–
$2\beta^+$	0ν	g.s.	511	8.85	16	$\geq 4.1 \times 10^{18}$	$\geq 3.5 \times 10^{17}$ [31]	$(5.2 - 9.6) \times 10^{31}$ [19, 42]
		g.s.	511	8.80	16	$\geq 4.1 \times 10^{18}$	$\geq 6.9 \times 10^{17}$ [26]	$(1.7-2.7) \times 10^{29}$ [19, 43, 44]
$^{138}\text{Ce} \rightarrow ^{138}\text{Ba}$								
$2K$	0ν	g.s.	616 ± 5	2.86	45	$\geq 4.7 \times 10^{17}$	$\geq 5.5 \times 10^{17}$ [31]	–
KL	0ν	g.s.	648 ± 5	2.82	25	$\geq 8.3 \times 10^{17}$	$\geq 4.6 \times 10^{17}$ [31]	–
$2L$	0ν	g.s.	679 ± 5	2.77	4.9	$\geq 4.2 \times 10^{18}$	$\geq 4.0 \times 10^{17}$ [31]	–

5. Conclusions

Deep purification of cerium oxide from radioactive contamination was obtained using the liquid-liquid extraction method. Measurements performed by ultra-low background γ -ray spectrometry have demonstrated a high efficiency of the purification method. The radiopurity of the CeO_2 sample is at the level of (less than) mBq kg^{-1} – tenths of mBq kg^{-1} of ^{137}Cs , ^{138}La , ^{139}Ce (cosmogenic radionuclide), ^{152}Eu , ^{154}Eu , ^{176}Lu , ^{226}Ra and γ -emitting daughters of ^{235}U . The activity of ^{238}U (estimated via ^{234m}Pa) does not exceed 12 mBq kg^{-1} , while ^{228}Ra and ^{228}Th remain in the sample at the level of 30 mBq kg^{-1} and 10 mBq kg^{-1} , respectively. Thus, the thorium concentration in the sample was reduced with this purification by a factor of 60. The purification protocol can be applied to produce radiopure cerium-containing crystal scintillators for the next stage experiments to search for double beta decay of cerium.

The experiment sets the best up-to-date limits on different modes and channels of double beta decay of ^{136}Ce and ^{138}Ce at the level of $T_{1/2} > 10^{17} - 10^{18} \text{ yr}$. The sensitivity of the experiment is still far from the theoretical predictions (given in Table 2). Further improvement of the experimental sensitivity can be achieved by using enriched materials, by further reduction of the background, and by the application of cerium-containing crystal scintillators to increase the detection efficiency.

References

- [1] J. Barea, J. Kotila, F. Iachello, Limits on Neutrino Masses from Neutrinoless Double- β Decay, *Phys. Rev. Lett.* 109 (2012) 042501.
- [2] W. Rodejohann, Neutrino-less double β decay and particle physics, *J. Phys. G* 39 (2012) 124008.
- [3] S. Dell’Oro, S. Marcocci, M. Viel, F. Vissani, Neutrinoless Double Beta Decay: 2015 Review, *AHEP* 2016 (2016) 2162659.
- [4] J.D. Vergados, H. Ejiri, F. Simkovic, Neutrinoless double beta decay and neutrino mass, *Int. J. Mod. Phys. E* 25 (2016) 1630007.
- [5] F.F. Deppisch, M. Hirsch, H. Päs, Neutrinoless double- β decay and physics beyond the standard model, *J. Phys. G* 39 (2012) 124007.

- [6] S.M. Bilenky, C. Giunti, Neutrinoless double- β decay: A probe of physics beyond the standard model, *Int. J. Mod. Phys. A* 30 (2015) 1530001.
- [7] V.I. Tretyak, Yu.G. Zdesenko, Tables of double β decay data – an update, *At. Data Nucl. Data Tables* 80 (2002) 83.
- [8] S.R. Elliott, Recent progress in double beta decay, *Mod. Phys. Lett. A* 27 (2012) 123009.
- [9] A. Giuliani, A. Poves, Neutrinoless Double-Beta Decay, *AHEP* 2012 (2012) 857016.
- [10] O. Cremonesi, M. Pavan, Challenges in Double Beta Decay, *AHEP* 2014 (2014) 951432.
- [11] J.J. Gómez-Cadenas, J. Martín-Albo, Phenomenology of Neutrinoless Double Beta Decay, *Proc. of Sci. (GSSI14)* 004 (2015).
- [12] X. Sarazin, Review of Double Beta Experiments, *J. Phys.: Conf. Ser.* 593 (2015) 012006.
- [13] M. Agostini et al., Background-free search for neutrinoless double- β decay of ^{76}Ge with GERDA, *Nature* 544 (2017) 47.
- [14] J.B. Albert et al. (The EXO-200 Collaboration), Search for Majorana neutrinos with the first two years of EXO-200 data, *Nature* 510 (2014) 229.
- [15] K. Alfonso et al. (CUORE Collaboration), Search for Neutrinoless Double-Beta Decay of ^{130}Te with CUORE-0, *Phys. Rev. Lett.* 115 (2015) 102502.
- [16] R. Arnold et al., Results of the search for neutrinoless double- β decay in ^{100}Mo with the NEMO-3 experiment, *Phys. Rev. D* 92 (2015) 072011.
- [17] A. Gando et al. (KamLAND-Zen Collaboration), Search for Majorana Neutrinos Near the Inverted Mass Hierarchy Region with KamLAND-Zen, *Phys. Rev. Lett.* 117 (2017) 082503.
- [18] J. Maalampi, J. Suhonen, Neutrinoless Double β^+ /EC Decays, *AHEP* 2013 (2013) 505874.

- [19] M. Hirsch, K. Muto, T. Oda, H.V. Klapdor-Kleingrothaus, Nuclear structure calculation of $\beta^+\beta^+$, β^+/EC and EC/EC decay matrix elements, *Z. Phys. A* 347 (1994) 151.
- [20] J. Bernabeu, A. De Rujula, C. Jarlskog, Neutrinoless double electron capture as a tool to measure the electron neutrino mass, *Nucl. Phys. B* 223 (1983) 15.
- [21] V.S. Kolhinen et al., On the resonant neutrinoless double-electron-capture decay of ^{136}Ce , *Phys. Lett. B* 697 (2011) 116.
- [22] J. Kotila, J. Barea, F. Iachello, Neutrinoless double-electron capture, *Phys. Rev. C* 89 (2014) 064319.
- [23] M. Doi, T. Kotani, Neutrinoless modes of double beta decay, *Prog. Theor. Phys.* 89 (1993) 139.
- [24] M. Wang et al., The AME2016 atomic mass evaluation, (II). Tables, graphs and references, *Chin. Phys. C* 41 (2017) 030003.
- [25] J. Meija et al., Isotopic compositions of the elements 2013 (IUPAC Technical Report), *Pure Appl. Chem.* 88 (2016) 293.
- [26] R. Bernabei et al., Feasibility of $\beta\beta$ decay searches with Ce isotopes using CeF_3 scintillators, *Nuovo Cimento A* 110 (1997) 189.
- [27] F.A. Danevich et al., Quest for double beta decay of ^{160}Gd and Ce isotopes, *Nucl. Phys. A* 694 (2001) 375.
- [28] P. Belli et al., Performances of a CeF_3 crystal scintillator and its application to the search for rare processes, *Nucl. Instrum. Meth. A* 498 (2003) 352.
- [29] P. Belli et al., Search for 2β decay of cerium isotopes with CeCl_3 scintillator, *J. Phys. G* 38 (2011) 015103.
- [30] P. Belli et al., First limits on neutrinoless resonant 2ε captures in ^{136}Ce and new limits for other 2β processes in ^{136}Ce and ^{138}Ce isotopes, *Nucl. Phys. A* 824 (2009) 101.
- [31] P. Belli et al., Search for double beta decay of ^{136}Ce and ^{138}Ce with HPGe gamma detector, *Nucl. Phys. A* 930 (2014) 195.

- [32] O.G. Polischuk et al., Purification of lanthanides for double beta decay experiments, AIP Conf. Proc. 1549 (2013) 124.
- [33] I. Kawrakow, D.W.O. Rogers, The EGSnrc code system: Monte Carlo simulation of electron and photon transport, NRCC Report PIRS-701, Ottawa, 2003.
- [34] S. Agostinelli et al., GEANT4 – a simulation toolkit, Nucl. Instrum. Meth. A 506 (2003) 250.
- [35] O.A. Ponkratenko, V.I. Tretyak, Yu.G. Zdesenko, Event generator DECAY4 for simulating double-beta processes and decays of radioactive nuclei, Phys. At. Nucl. 63 (2000) 1282.
- [36] V.I. Tretyak, in preparation.
- [37] A.A. Sonzogni, Nuclear Data Sheets for A = 136, Nucl. Data Sheets 95 (2002) 837.
- [38] G.J. Feldman, R.D. Cousins, Unified approach to the classical statistical analysis of small signals, Phys. Rev. D 57 (1998) 3873.
- [39] M.I. Krivoruchenko et al., Resonance enhancement of neutrinoless double electron capture, Nucl. Phys. A 859 (2011) 140.
- [40] J. Suhonen, Nuclear matrix elements for the resonant neutrinoless double electron capture, Eur. Phys. J. A 48 (2012) 51.
- [41] O.A. Rumyantsev, M.H. Urin, The strength of the analog and Gamow-Teller giant resonances and hindrance of the $2\nu\beta\beta$ -decay rate, Phys. Lett. B 443 (1998) 51.
- [42] J. Abad, A. Morales, R. Nunez-Lagos, A.F. Pacheco, An estimation of the rates of (two-neutrino) double beta decay and related processes, J. Physique 45 (1984) C3-147.
- [43] J. Barea et al., Neutrinoless double-positron decay and positron-emitting electron capture in the interacting boson model, Phys. Rev. C 87 (2013) 057301.
- [44] J. Suhonen, M. Aunola, Systematic study of neutrinoless double beta decay to excited 0^+ states, Nucl. Phys. A 723 (2003) 271.